Received: 5 December 2022 | Revised: 30 March 2023 | Accepted: 30 April 2023

DOI: 10.1002/eco.2556

RESEARCH ARTICLE

WILEY

Impact of shading on evapotranspiration and water stress of urban trees

Laura Tams | Eva Nora Paton | Björn Kluge

Department of Ecohydrology, Institute of Ecology, Technische Universität Berlin, Berlin, Germany

Correspondence
Laura Tams, Department of Ecohydrology, Institute of Ecology, Technische Universität Berlin, Berlin, Germany.
Email: l.tams@tu-berlin.de

Funding information
Deutsche Forschungsgemeinschaft; Federal Ministry for the Environment, Nature Conservation, Nuclear Safety and Consumer Protection

Abstract

Evapotranspiration of urban street trees is essential in mitigating urban heat islands due to its cooling effect. However, current shifts in rainfall and temperature regimes towards drier and hotter periods in Central Europe have caused substantial water stress for street trees. Quantifying and subsequently managing these changing dynamics as well as estimating evapotranspiration and water availability is necessary but at the same time extremely challenging in urban environments. Both dynamics are influenced by soil sealing and complex shading patterns of the surrounding street canyon, which vary on a small spatial scale as a function of the canyon layout and orientation. In the present study, the diurnal patterns of six typical urban shading types for street trees were derived by considering a large set of street orientations, widths and tree positions within the street canyon. A shading model was integrated into a hydrological urban tree model to assess the impact of those shading types on diurnal patterns of radiation and evapotranspiration rates calculated using the Penman–Monteith approach and the resulting soil moisture conditions for several vegetation seasons and water-supply scenarios. The modelling results showed that the six shading patterns significantly influenced the simulated hourly, daily and seasonal potential and actual evapotranspiration rates and water availability. Shaded trees have a substantially reduced, simulated water stress period, regardless of initial water supply, and are able to provide a longer-lasting cooling function during dry periods due to higher evapotranspiration rates later in the summer season.

KEYWORDS
diffuse radiation, direct radiation, evapotranspiration (ET), global radiation, shading, urban environment, urban trees, water stress

1 | INTRODUCTION

Urban ecohydrology remains of great interest due to the complex interactions of the heterogeneous built environment and the urban vegetation. Street trees in highly dense areas are of specific interest, as they are exposed to significantly different shading patterns (Gong et al., 2019) and high water stress during dry periods. In temperate zones, street trees are particularly vulnerable to summer heat waves and extended dry periods due to their limited adaption (Haase & Hellwig, 2022). The consequences of water stress are manifold, including limited tree growth (Rötzer et al., 2019), fitness and life expectancy (Bréda et al., 2006; Haase & Hellwig, 2022), reduced evapotranspiration (Rahman et al., 2017; Rötzer et al., 2021) and cooling potential (Adams et al., 2012; Bowler et al., 2010). Current

measures, such as manual irrigation, are limited and only applied during extreme conditions in temperate zones in Central Europe (David et al., 2018; Dickhaut & Eschenbach, 2018; SenUVK, 2021). To improve irrigation management and avoid the risk of vitality losses and mortality of urban trees, it is necessary to clearly understand urban tree water demand, considering shading patterns and site-specific effects (McDowell et al., 2008; Schütt et al., 2022; Wessolek & Kluge, 2021).

Microclimatic studies demonstrate that within a street canyon, short-wave radiation, both diffuse and direct components, is strongly influenced by shading (Mei & Yuan, 2022). To characterize shading within street canyons, the sky view factor (SVF) is used to describe the reduction in diffuse radiation by the ratio of built-up area to open sky (Johnson & Watson, 1984). A different binary approach additionally reduces the direct radiation to zero during shading periods (Gong et al., 2019; Ross, 1981). With the binary approach, it is possible to include the effects of shading based on street canyon orientation, sun elevation, building height and tree position.

Evapotranspiration (ET) is a key variable to quantify water flow and stress at the atmosphere–soil–plant interface (Allen et al., 2006; Olmedo et al., 2016). In many urban tree models, evapotranspiration is also used to evaluate the general cooling effect (Pace et al., 2021), including a reduction of global radiation (Grylls & van Reeuwijk, 2021; Hörnschemeyer et al., 2021; Wessolek & Kluge, 2021) or the occurrence of water stress (Revelli & Porporato, 2018; Rötzer et al., 2021; Vico et al., 2014). To our best knowledge up to date, no monitoring study has quantified the effects of shading on the water stress of street trees. For example, Vico et al. (2014) estimated the daily cooling capacity and irrigation needs of individual street trees, accounting for soil water storage, tree water requirements and different growing conditions. However, the effects of shading on evapotranspiration were not considered in calculating the water balance. Wessolek and Kluge (2021) developed hydro-pedotransfer functions (HPTFs) to calculate the annual water demand, potential ET (ETp), actual ET (ETa) and water stress of street trees. The function applies to different tree ages, species, soil sealings, soil types and global radiation is reduced with the SVF. The HPTFs provide a good approximation of the annual water balance of street trees. However, the critical water stress periods during the vegetation period cannot be identified. Finally, Hörnschemeyer et al. (2021) used the SWMM model to quantify the effect of shading on ETa for urban conifer areas by employing a shade factor that reduces ETa depending on monthly solar elevation.

In conclusion, existing water models for urban trees do not (Vico et al., 2014) or only partially include the effects of shading (Hörnschemeyer et al., 2021; Wessolek & Kluge, 2021). None of the studies considered varying shading patterns typically found within street canyons, which affect global radiation and potential evapotranspiration on a diurnal time scale. Therefore, we argue that different diurnal shading types need to be developed. Through this study, the effects of the shading patterns on the water balance of street trees were evaluated to identify the critical timeframes and site conditions for water stress in the urban environment.

We hypothesized that the daily and seasonal evapotranspiration rates are significantly influenced by shading and that street trees exposed to direct radiation experience considerably larger and longer lasting water stress than shaded trees. Therefore, by applying the contrario argument, shaded trees should be better adapted to heat and drought periods and may also provide their cooling function more efficiently than exposed trees. To test these hypotheses, the following objectives were formulated: We (i) conceptualized typical urban shading types for street trees, (ii) quantified the impact of the various shading types on diurnal patterns of global radiation and potential evapotranspiration as a function of different sky conditions, (iii) quantified the impact of the urban shading types on actual evapotranspiration and soil moisture rates comparing three cases, 'well-water-supplied', a 'drought-induced' and a hypothetical 'legacy effect' throughout the vegetation period of four recent years, and (iv) assess the impact of typical urban soil sealing for the three cases.

2 | METHODS

2.1 | Urban tree model

To determine the effect of shading on the water supply, a hydrological model (URbanTRee; Figure 1), including extensions and adaptions for individual street trees in typical urban settings, was further developed after preliminary work by Kirmaier (2020). URbanTRee calculates potential and actual water losses by evapotranspiration on an hourly time step based on the Penman–Monteith equation (Allen et al., 2006) using a subroutine of the R package 'Water' created by Olmedo et al. (2016) combined with a bucket model to calculate the soil moisture storage in the upper soil zone in R, version 4.1.2 (R Core Team, 2021). Moreover, it includes routines for interception derived after (Gash, 1979), infiltration calculation based on a constant runoff factor and percolation losses (all model equations of the URbanTRee model are given in Appendix A). The model domain of URbanTRee is given by the crown size and a model layer defined by the rooting depth of the street tree. URbanTRee considers the heterogeneous functioning of urban surfaces, such as open tree pits, pavement and asphalt surfaces, and calculates runoff, infiltration and changes to soil water storage separately for each surface and associated storage fraction.

2.2 | Urban shading submodel

The ShadingType submodel was integrated into the URbanTRee model by decreasing both parts of the global radiation rate (R_G), direct radiation (R_D) and diffuse radiation (R_{Diff}), to calculate ET during shading hours:

$$R_G = \begin{cases} R_{Diff} \times SVF & \text{for shading} \\ R_{Diff} \times SVF + R_D & \text{for no shading} \end{cases} \left(\mathrm{Wm}^{-2}\right) \quad (1)$$

Direct radiation R_D is reduced to zero during shading hours, whereas diffuse radiation R_{Diff} is reduced by the SVF, which can take values between zero and one and varies depending on the density of

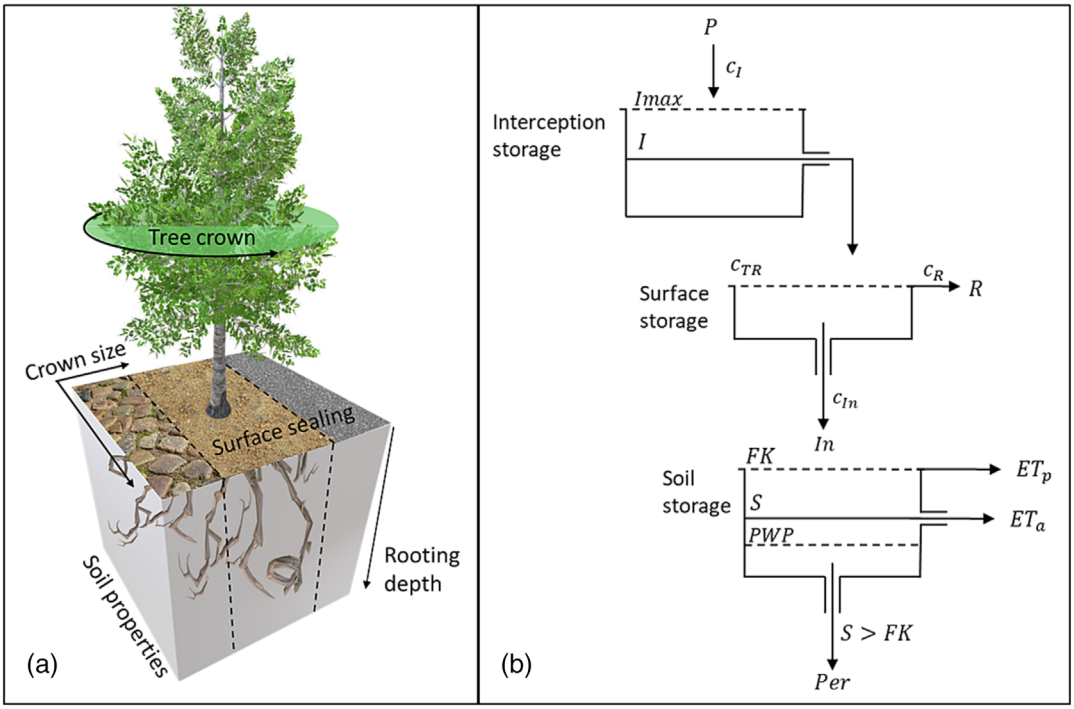

FIGURE 1 Conceptual representation of the URbanTRee spatial setup (a) and the schematic diagram (b) of the key processes (P, precipitation; I, interception; R, runoff; In, infiltration; S, soil moisture; Per, percolation; ETp, potential evapotranspiration and ET_a, actual evapotranspiration).

surrounding buildings (Johnson & Watson, 1984). Direct radiation was calculated by subtracting the diffuse radiation rate from the global radiation rate. The binary approach by Gong et al. (2019) (Equation 1) suggests a significant improvement of shading representation. To verify the modelling approach, data from a shaded and non-shaded SPN1 global and diffuse radiation pyranometer (Delta-T Devices, 2022) were compared with the modelling results. Subsequently, hourly time series for diffuse and global radiation were used for calculation (DWD Climate Data Center, 2022).

2.2.1 | Identification of diurnal shading types

The geometric alignment of typical urban properties and sun elevation was used to identify typical urban shading types. Hourly shading patterns were derived for four different street orientations, a wide and narrow street, and for tree positions on either side of the street. The sun elevation (α) and angle of the vector 'building-top to tree-reference-height' (β) are being compared:

$$\beta(\gamma) = atan((H-h)/D)\,(^\circ) \tag{2}$$

where H is the building height (m), h is the tree reference height (m) and D is the distance from the building (m) (Figure 2). The temporal change in azimuth (γ) was included in the calculation of the two angles:

$$f(\gamma) = \begin{cases} 0 \text{ for } \alpha < \beta \\ 1 \text{ for } \alpha > \beta \end{cases}(^\circ) \tag{3}$$

To calculate the azimuth and solar elevation, the R-package 'solarPos' was used (Doninck, 2016). Here, the building height is defined by a typical Berlin eaves height of 22 m (Böhme et al., 2020), and the tree reference height refers to the midpoint of the tree crown, which was assumed to be 3 m. For simplification, we considered trees to be completely shaded or completely exposed to sunlight.

2.3 | Input data and model parametrization

Hourly climate input data used originated from the secular station Berlin–Potsdam (DWD Climate Data Center, 2022). In Berlin, the climate is described as warm temperate and humid continental (Köppen and Geiger: Cfb after Kottek et al., 2006), with an average precipitation sum of 570 mm/year. In this study, the period 2017–2020 was analysed, with above-average precipitation in 2017 (746 mm/year), extreme low precipitation in 2018 (345 mm/year) and two average years (542 mm in 2019 and 499 mm in 2020). Additionally, 2019 had a particular hot summer (DWD Climate Data Center, 2022).

The model was parametrized for the most abundant tree species in Berlin, *Tilia cordata* (SenUVK, 2021), more specifically for a *T. cordata* with an age of 15–30 years, a crown size of 16 m^2, a rooting depth of 1.5 m and a crop coefficient of K_C = 1.4–1.6 (Wessolek &

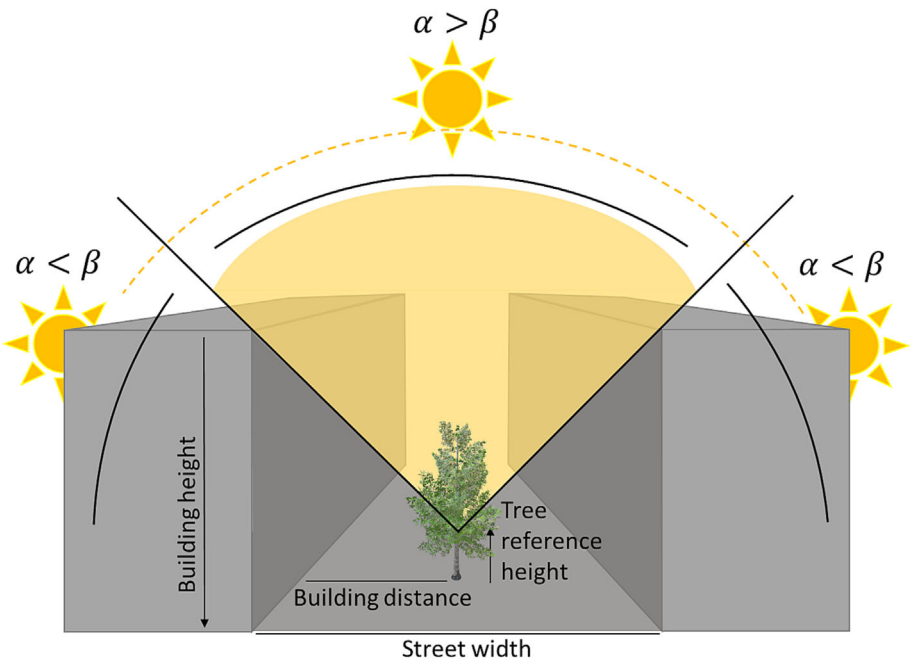

FIGURE 2 Schematic illustration of sun path (α) and street geometry (vector building-top to tree-reference-height, β) effecting shading patterns: shading occurs when α < β.

Kluge, 2021). The pheno-multiplier ($c_P = 0.5$, for first 2 weeks of leaf development and last 2 weeks of leaf shedding) was added to describe the stage of development throughout the vegetation period. Further, the evapotranspiration is reduced by 50% according to the water stress coefficient (K_{EA}) if the usable field capacity falls below 30% (water stress factor $K_S = 0.3$). At the permanent wilting point (PWP), plant water is no longer available in the soil, and the evapotranspiration is reduced to zero.

Tree pit characteristics can vary strongly in size, soil sealing degree and substrate. In this model, the soil texture is defined as a weak loamy sand (Sl2), which is typical for Berlin centre located in the glacial valley 'Berliner Urstromtal' (SenUVK, 2018). The parameter field capacity (FK) and the PWP were determined according to the soil physical reference database of Wessolek et al. (2009). The mean FK and the PWP of a loamy sand (Sl2) with a bulk density of 1.4 g cm^{-3} are 26 and 10 m^3m^{-3}, respectively; capillary rise from groundwater was assumed not to occur. The tree pit size in turn corresponds to the unsealed part of the catchment area, which is defined as 100% open soil and 100% asphalt surface sealing, resulting in a tree pit size of 16 and 0 m^2 respectively. All parameterization values are again summarized in Appendix A (Table A2).

2.4 | Model scenarios for the analysis of shading impact

Different modelling approaches were applied to investigate the influence of urban shading types on global radiation, ETp and ETa rates and soil moisture.

First, the effects of shading on global radiation (Equation 1) and ETp (Equation 4) were investigated by comparing different degrees of cloud cover in spring (April) and summer (June) of 2017–2020. Cloud cover was categorized into clear sky (diffuse radiation <20% of global radiation), cloudy sky (diffuse radiation 20%–80% of global radiation) and grey sky (diffuse radiation >80% of global radiation). Diurnal variations on an hourly basis were compared to identify urban shading patterns. Moreover, the daily sums provided insight into the differences among the different shading patterns throughout the entire vegetation period (2020).

Second, the effects of shading on ETa and soil moisture were quantified over the course of four vegetation periods with different yearly precipitation sums (2017–2020). Comparing the shading types, in the respective year, the first dry day of the year (FDD), sum of dry days (SDD) and yearly ETa sum during the vegetation period were considered. A dry day was defined as a day wherein the inferior limit of available water in the soil was reached, that is, the permanent wilting point (PWP, 10 m^3m^{-3}).

Three case studies were investigated by regulating soil moisture at the beginning of the vegetation period (1 of April): 'well water supplied' with good initial starting conditions for plant available water (FK: 26 m^3m^{-3} soil moisture), 'drought induced' with a generated water stress with dry initial starting conditions (16 m^3m^{-3} soil moisture, the threshold of a loamy sand for beginning water stress, defined in equation (10) (Appendix, Table A1), derived from Wessolek et al. (2009)), and 'legacy effect' was used to examine replenishment processes during a continuous model run (2017–2020) with a soil moisture content of 26 m^3m^{-3} at the beginning of 2017. The impact of snowmelt was not considered.

At last, to quantify the impact of soil sealing, the three case studies were performed with 100% open soil catchment and 100% sealed surface catchment (with asphalt).

3 | RESULTS

3.1 | Identification of urban shading types

The simulation to identify typical urban shading types was performed for different months during the vegetation period, but no substantial differences were observed. In the 16 scenarios, the sun position resulted in different shading patterns (Figure 3), which were clustered into six groups: sun all day (≥9 h), no sun (≤2 h), afternoon sun (3–5 h, after 13:00), morning sun (3–5 h, before 13:00), midday sun (3–5 h, after 10:00 and before 15:00) and morning and evening sun (>2 h, before 10:00 and after 15:00).

By applying the urban shading model, the global radiation was reduced during the shaded hours. Figure 4 shows that the diurnal pattern of global radiation for a shaded site (in the morning and early afternoon) is better represented by the values of the shading model compared to the values of the non-shaded site.

In combining the diurnal shading patterns with the reduction in global radiation, six typical urban shading scenarios were defined: A: sun all day, B: no sun all day, C: shade before noon (5 AM–1 PM), D: shade in the afternoon (1–8 PM), E: shade in the morning and evening (8–10 AM and 3–8 PM) and F: shade at noon (10 AM–2 PM) (Figure 5).

3.2 | Impact of shading on global radiation and potential evapotranspiration rates

Compared to the non-shaded type A, a clear reduction in global radiation and potential evapotranspiration (ETp) was visible for all other shading types on days with clear skies (Figure 6). The reduction was most pronounced for type B (all-day shadow) and affected the diurnal cycle of the other scenarios as a function of their shading hours. This distinction was substantially smaller on cloudy days and unnoticeable on grey days. When comparing spring to summer, the diurnal patterns of the global radiation were 100–150 W/m^2 higher in summer for scenarios A and C–F. The ETp values for all shading types were 0.15–0.25 mm higher in summer than in spring.

Considering the daily cumulative global radiation and daily sum of ETp during the entire vegetation period (Figure 7), the global radiation of shading type A on clear sky days was seven times higher than that of type B and two to three times higher than that of types C–F. On cloudy days, type A was up to three times higher than types B–F, and on grey sky days up to two times.

The difference in ETp was less evident; however, the mean ETp was still two times higher for type A compared to type B and 1.3–1.6 times higher compared to types C–F. On cloudy and grey sky days, the difference between all shading types compared to A was negligible.

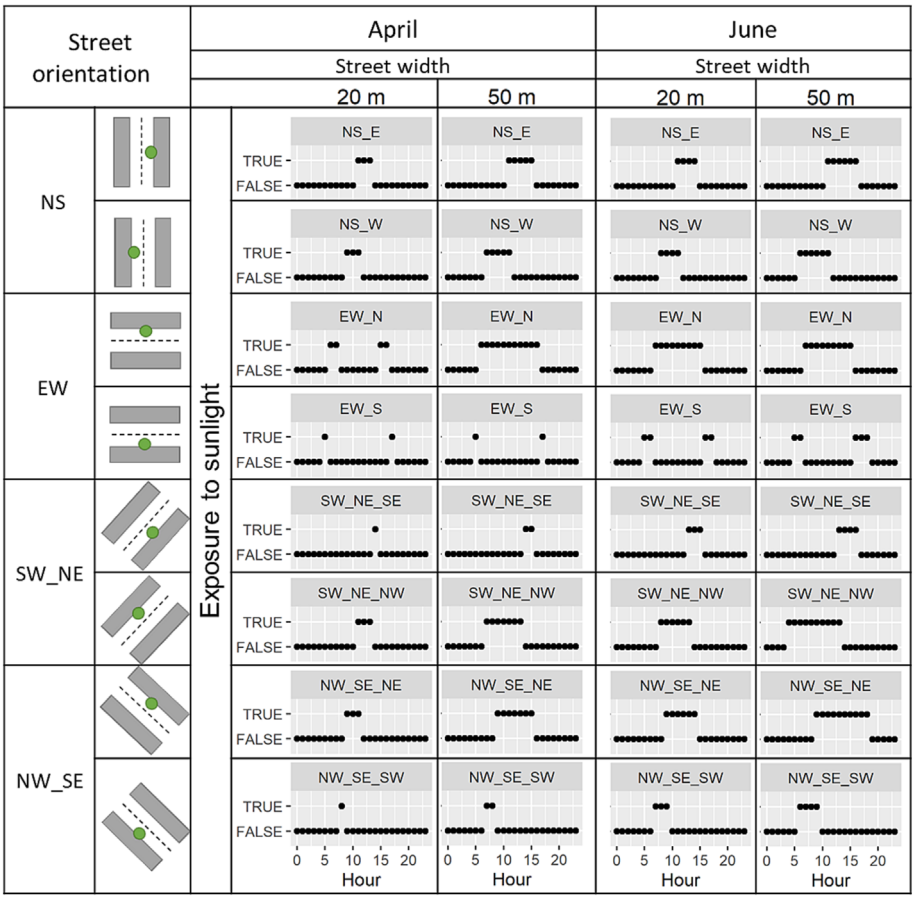

FIGURE 3 Shading patterns for 16 different urban settings in April and June. True indicates exposure to sunlight, and false the shaded hours.

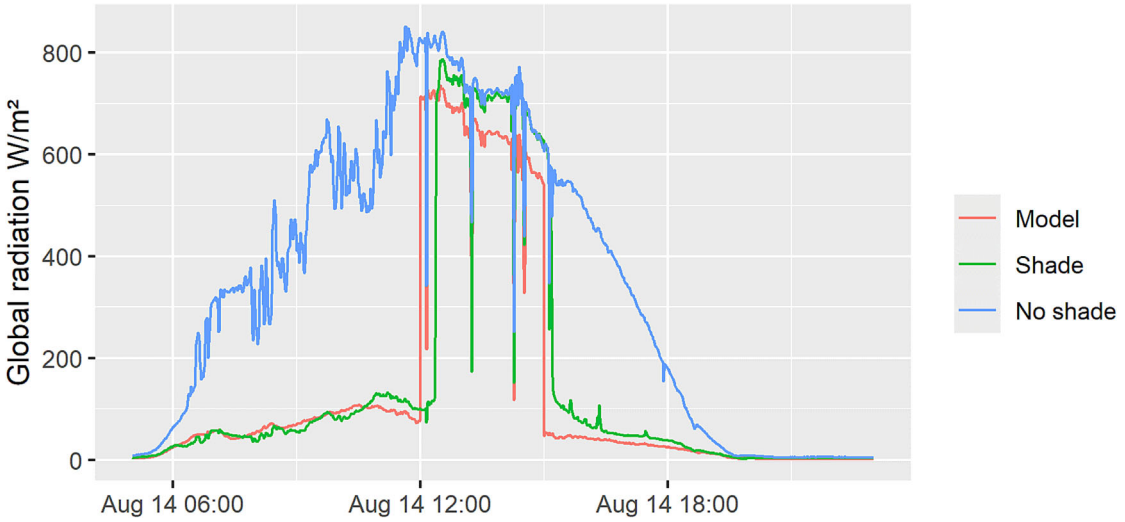

FIGURE 4 Global radiation rates for the urban shading model (Model), the monitoring site with shading in the morning and afternoon (Shade) and the monitoring site without any shading (No shade). The measurements were made with SPN1 sunshine pyranometer (Delta-T Devices, 2022).

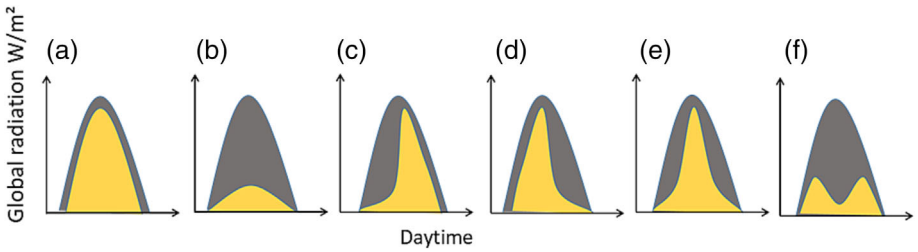

FIGURE 5 Schematic diurnal variations of global radiation for six typical urban shading types: (a) no shade, (b) shade all day, (c) shade before noon (5 AM–1 PM), (d) shade in the afternoon (1–8 PM), (e) shade in the morning and evening (8–10 AM and 3–8 PM), (f) shade at noon (10 AM–2 PM).

3.3 | Impact of shading on actual evapotranspiration rates and soil moisture dynamics

3.3.1 | Comparisons within the open soil 'well water supplied' case

Modelling results showed that actual evapotranspiration (ETa) was highest for type A (up to 10 mm/day) and lowest for type B (up to 7 mm/day) at the beginning of the growing season (April) (Figure 8). Throughout the vegetation period, the dynamic changes, as the water content for type A decreased more rapidly than for type B. ETa remained higher for fully shaded type B when the soil moisture of type A fell below 15 m^3m^{-3} (mid-May) or the PWP was reached (beginning of June). Zooming into the ETa plot, dynamic changes among the orders of shading types C–F are observed. Zooming in to the soil moisture plot on the other hand, the order of shading types C–F did not change (Figure 8, zoom).

The first dry day (FDD) in shading type A occurred between the 150th and 170th day of the year (DOY) (Figure 11). In comparison, in type B, the FDD was reached up to 5 weeks later (2019). For shading types C–F, the FDD occurred with delay of 1–5 weeks in comparison to type A. In 2017, no dry day occurred for shading types B, D, E and F.

The highest sum of dry days (SDD) was observed for type A, with significant variations from 16 to 80 SDD in 2017 and 2018, respectively. Type B showed the highest deviation in SDD compared to type A and experienced 3 weeks less water stress in 2018. The smallest variation of SDD was 1 week less for type C in 2019, and the average deviation was 12 days less for types B–F.

The sums of ETa for all six shading types showed only minor a differences of approximately 10–20 mm (2018–2020) and up to 40 mm (2017), even though their temporal patterns during the course of the year differed from one another considerably (Figure 11).

3.3.2 | Comparisons within the open soil 'drought-induced' case

In the water-stressed case, the modelling results showed significantly reduced ETa rates for all shading types, with a maximum ETa of approximately 5 mm/day. The highest ETa values were mainly found in shading type A, and only when the permanent PWP was reached (mid-May), ETa was higher for shading type B (Figure 9).

In all years, the FDD was reached between the 135th–150th DOY in shading type A and up to 2 months later in type B (2020) (Figure 11). On average, shading types B–F reached the FDD 1–12 days later than type A.

The SDD in shading type A ranged between 25 (2017) and 90 (2018) days, and the SDD in B-F was on average 12 days

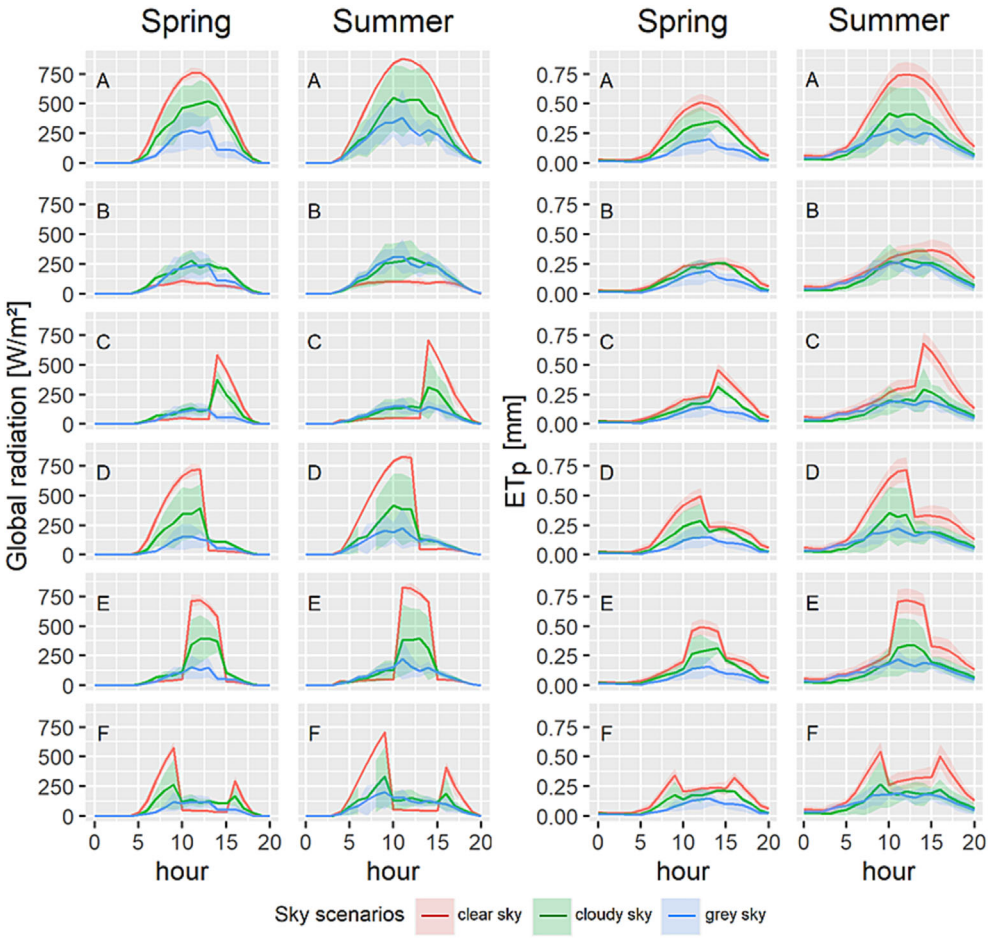

FIGURE 6 Effect of shading on global radiation and potential evapotranspiration (ETp) in spring and summer for three cloud conditions: clear sky (diffuse radiation <20% of global radiation), cloudy sky (diffuse radiation 20%–80% of global radiation) and grey sky (diffuse radiation >80% of global radiation) for six typical urban shading types: A: no shade; B: shade all day, C: shade before noon, D: shade in the afternoon, E: shade in the morning and evening, F: shade at noon.

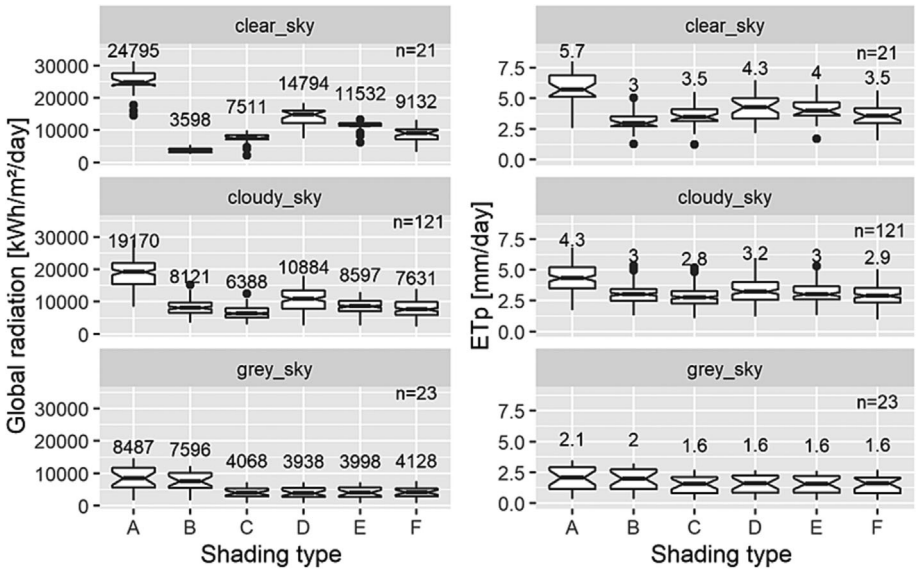

FIGURE 7 Daily sum of global radiation (left) and potential evapotranspiration (ETp, right) for typical urban shading types: A: no shade; B: shade all day, C: shade before noon, D: shade in the afternoon, E: shade in the morning and evening, F: at noon, exemplarily for the vegetation period April–September 2020 for three cloud amounts: clear sky (diffuse radiation <20% of global radiation), cloudy sky (diffuse radiation 20%–80% of global radiation) and grey sky (diffuse radiation >80% of global radiation).

shorter. The highest deviation in SDD occurred, with 1 month less, in type B (2020) and the lowest, with 5 days less, in type D (2020).

Again, the ETa sum showed no significant difference between shading types, although the temporal occurrences were rather different (Figure 11).

3.3.3 | Comparisons within the open soil 'legacy effect' case

In the continuous case study, the maximum daily ETa reached 10 mm/day in shading type A after full leaf development in 2017 and 2018. Shading types B–F did not reach 10 mm/day in any year

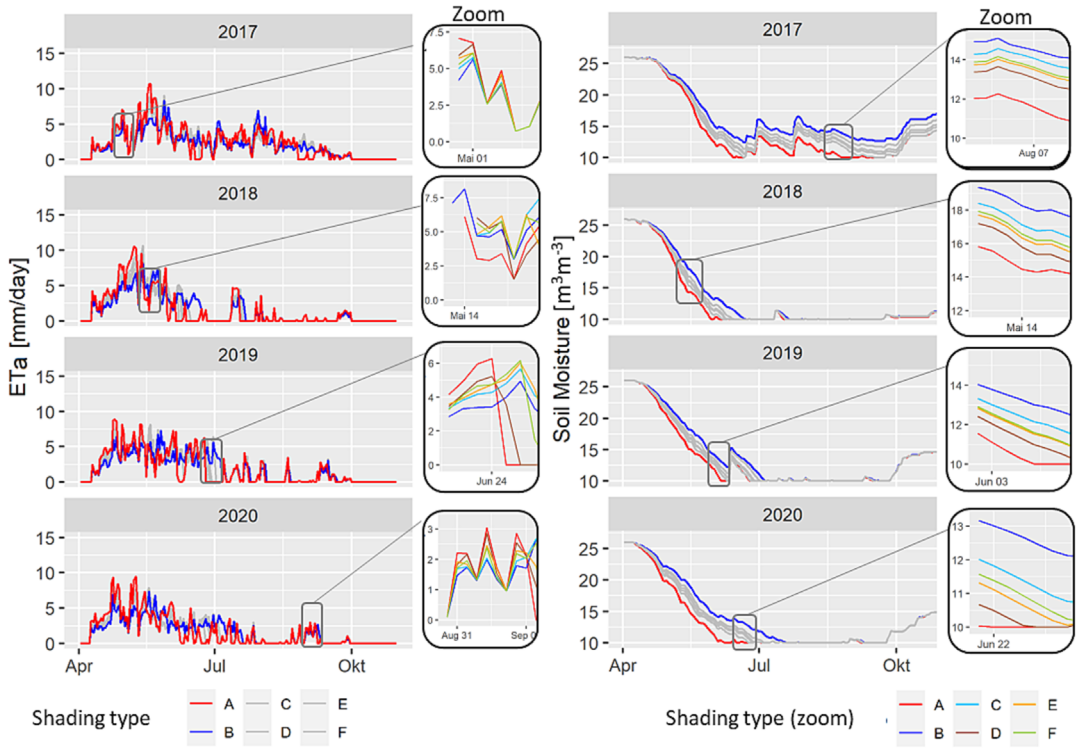

FIGURE 8 Daily sum of actual evapotranspiration (ETa) and soil moisture content for the open soil 'well water supplied' case for typical urban shading types: A: no shade; B: shade all day, C: shade before noon, D: shade in the afternoon, E: shade in the morning and evening, F: shade at noon. The period 2017–2020 was simulated using data from Potsdam weather station (DWD Climate Data Center, 2022). Note: For the zoomed portions, a second legend is provided on the bottom right.

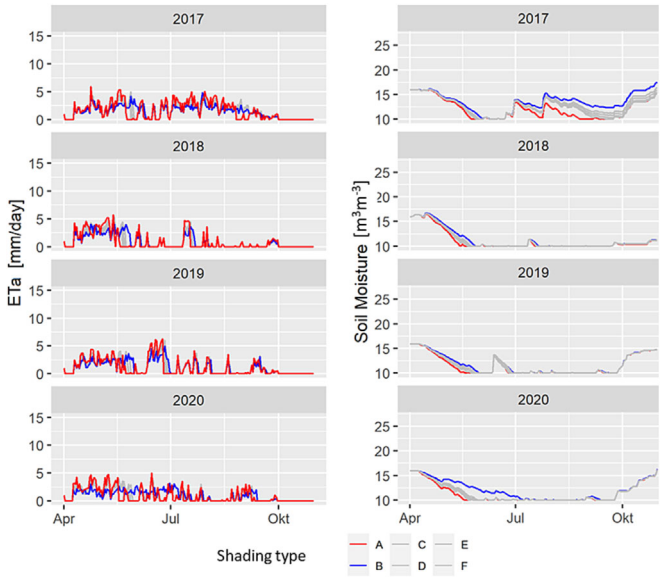

FIGURE 9 Daily sum of actual evapotranspiration (ETa) and soil moisture content for the open soil 'drought-induced' case for typical urban shading types: A: no shade; B: shade all day, C: shade before noon, D: shade in the afternoon, E: shade in the morning and evening, F: shade at noon. The period 2017–2020 was simulated using data from Potsdam weather station (DWD Climate Data Center, 2022).

(Figure 10). However, shading types B–F periodically reached higher ETa rates in comparison to shading type A during dry periods in all years. A different visualization method was used to enable a better interpretation of legacy effects regarding water conditions from previous seasons. The soil moisture content in April 2019 was much lower than that in the other years because of the dry conditions in 2018 and a shorter replenishment phase. However, we did not find a significant difference between the six shading types when comparing the soil moisture at the beginning of the vegetation period 2019 (differ by 0.1–0.2 m^3m^{-3}).

The FDD in shading type A occurred around the 150th–170th DOY, and in shading types B–F around 2–6.5 weeks later (Figure 11). The SDD in type A varied from 16 (2017) to 80 days (2018); in comparison, for shading types B–F, the water stress was on average 17 days shorter. The highest divergence, with 3 weeks less, occurred in type C (2019), and the lowest, with 2 weeks less, occurred in type D (2020). Furthermore, the ETa sum showed no significant difference between the shading types, but the temporal patterns differed among them (Figure 11).

3.3.4 | Combined impact of soil sealing and shading on evapotranspiration and soil moisture

A fully sealed soil with asphalt around the tree crown area was expected to cause an earlier start of the dry period and a longer exposure to dry conditions in comparison to a tree in open soil. Figure 11 compares multiple model runs: an open soil (triangle) and an asphalt surface sealing (circle), summarizing the FDD, SDD and ETa sum for all three model case studies (well-watered, drought-induced and

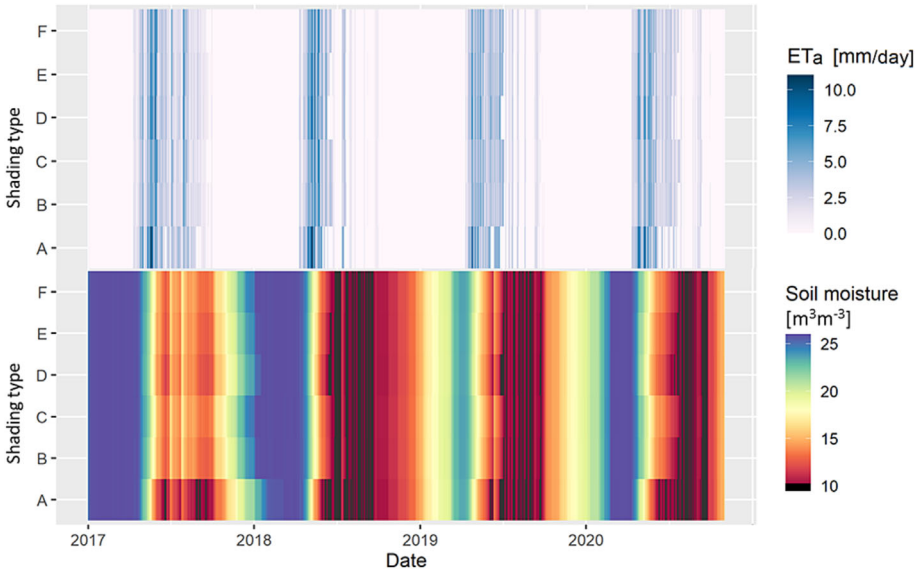

FIGURE 10 Daily sum of actual evapotranspiration (ETa) and soil moisture content for the open soil 'legacy effect' case for typical urban shading types: A: no shade; B: shade all day, C: shade before noon, D: shade in the afternoon, E: shade in the morning and evening, F: shade at noon. The period 2017–2020 was simulated using data from Potsdam weather station (DWD Climate Data Center, 2022).

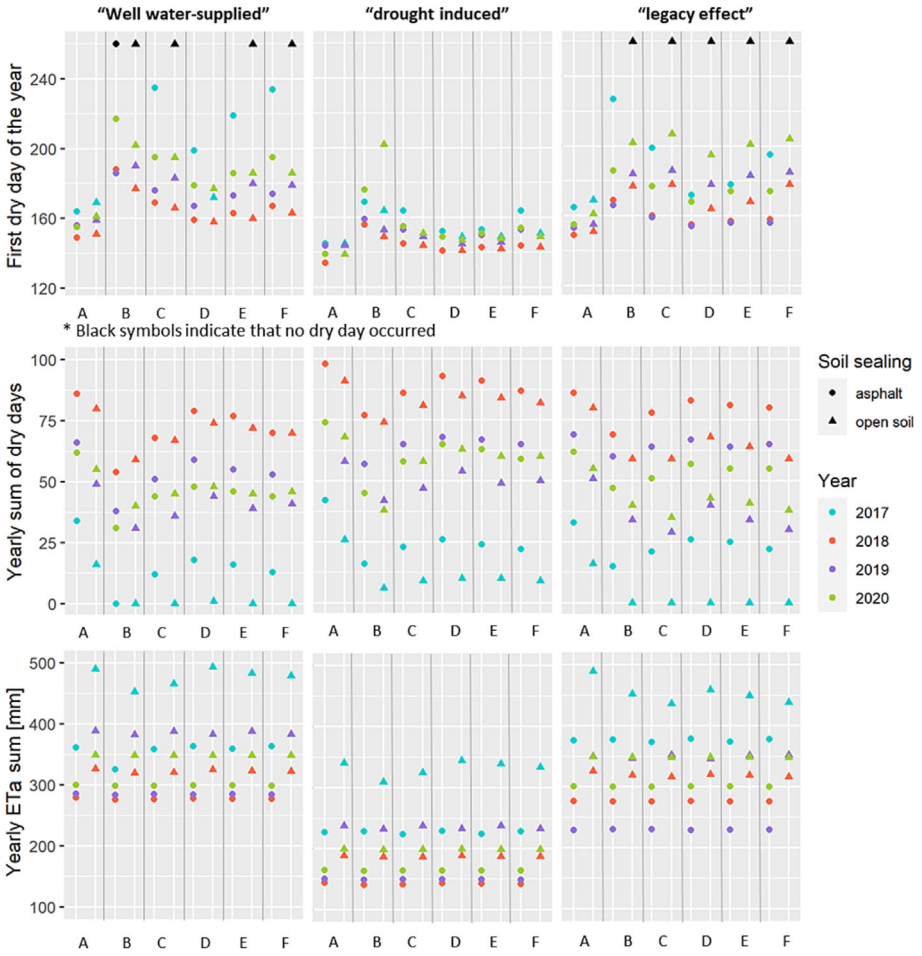

FIGURE 11 First dry day of the year (FDD), sum of dry days (SDD) and the ETa sum during the vegetation period of 'well water supplied' case study, a 'drought-induced' case study and a 'legacy effect' case study for typical urban shading types: A: no shade; B: shade all day, C: shade before noon, D: shade in the afternoon, E: shade in the morning and evening, F: shade at noon as well as an open soil and a sealed soil with asphalt condition during four different years. Simulated are four years (2017, 2018, 2019, 2020) using data from Potsdam weather station (DWD Climate Data Center, 2022).

legacy effect) and four different years (different colours for 2017–2020). In summary, the SDD was larger and the ETa sum was smaller for the asphalt sealing than for the open soil runs.

Soil sealing showed a particularly large effect for the wet year 2017 in the 'legacy effect' case, where FDD was significantly later in the runs with open soil than in the asphalt scenario for all shading scenarios, except for the non-shaded type A. The sealing shows very little effect on FDD in the 'drought-induced' case. Most pronounced again for the wet year 2017, but also visible for most of the other years, the SDD is larger for the asphalt than for the open soil sealings.

Finally, the ETa sum is lower for all asphalt simulations in comparison to the open soil simulations, and this impact was highest in the 'legacy effect' case.

4 | DISCUSSION

A modelling approach was used to evaluate cascading effects of shading on global radiation rates, modelled ETp, ETa and soil moisture availability for urban street trees under different climatic conditions. The model output clearly indicated the impact of different shading types on simulated water availability of street trees in all three case studies (well water supplied, drought-induced and legacy effect). Comparing the beginning of the water stress period of shading types B–F to shading type A, the response was least pronounced in the well water supplied case study with a delay of 1–12 days and most pronounced in the drought-induced case study with a of 2–8 weeks. Although there were minor differences in the yearly ETa sums, the seasonal distribution of ETa was significantly influenced by shading: shading type A showed higher ETa than shading types B–F at the beginning of the growing and summer season, whereas shading types B–F frequently had higher values towards the end of the growing season, when they still had water available for transpiration. These ETa patterns were found in all three cases studies (well water supplied, drought-induced and legacy effect).

We intended to use our modelling approach for hypothesis building, being aware that there are currently no available datasets to test the dynamics of transpiration rates of urban streets trees as a function of shading. Monitoring costs and labour are considered extremely high to equip urban trees under different shading and sealing conditions, ideally with several replica, potentially considering different tree ages and species, with soil moisture probes (for different depths), sap flow sensors and the full set of climatic sensors, including global and diffuse sensors (which are particularly costly) required for the quantification of ETp and ETa. However, to contextualize our modelling results, a comparison of the unshaded tree (shading type A) to measured annual evapotranspiration values of a 35-year-old tree by Wessolek and Kluge (2021) showed good agreement, with 320 versus 388 mm in 2019 and 340 versus 334 mm in 2020. Moreover, we use these modelling results to guide subsequent, future monitoring campaigns of water stress for street trees. The modelling results suggest to focus on the monitoring of hourly to sub-hourly rates of direct and global radiation, sap flow and soil moisture for trees whose shadow patterns match the six typical urban shading types to enable the analysis of their interlinked diurnal patterns and to validate or dismiss our findings regarding long-term water stress behaviour, ideally for vegetation periods of climatically different years.

4.1 | Uncertainties

In our model, we used a soil hydrological modelling approach, which takes a completely different perspective on ETa calculation than micro-meteorological models (Robineau et al., 2022). The majority of micro-meteorological models for urban water and surface energy balances yield good temperature estimates within the urban canopy but have a poor representation in terms of hydrological processes (Järvi et al., 2011). The evapotranspiration flux is widely assumed to be proportional to the air-specific humidity gradient between the surface and a reference level (Masson, 2000), but the latter is provided by the meteorological model itself (Berthier et al., 2006). On the other hand, the effect of shading is presented in a better fashion, as they consider its effects not only on radiation but also on surface temperature, wind patterns and resulting air temperature within a street canyon (Mei & Yuan, 2022) as a function of aspect ratios, orientation and building materials (Athamena et al., 2018; Chen et al., 2020). It remains a challenge to couple hydrological and micro-meteorological models. One of the first attempts were made by Robineau et al. (2022) who described the effect of water stress of a street tree on the surrounding climatic conditions, but not the effect vice versa.

To adequately represent the impact of trees on the urban environment, the canopy reference area is a conversely discussed parameter (Wang et al., 2021). It can be represented by the leaf area index, single-layer or multi-layer approaches (Gkatsopoulos, 2017; Grylls & van Reeuwijk, 2021; Wessolek & Kluge, 2021). In our model, we used the horizontal canopy area (single-layer approach) as the reference for ET calculations. The single-layer reference indicates that, at a given hour, only part of the tree actively participates in transpiration. As a result, no further partial-shading scenarios were included in this evaluation—an assumption that might need further evaluation beyond this study.

4.2 | Future research

The results suggest that shading can be an advantage as it results in delayed and lower water stress and thus helps to provide a longer lasting cooling effect throughout the vegetation period. In evaluating the influence of shade in this study, we focused primarily on soil moisture and the resulting actual evapotranspiration of trees. Nevertheless, in future research, all benefits and detriments of shading need to be discussed in terms of CO_2 storage and biomass production (Rötzer et al., 2019), cooling capacity (Rahman et al., 2017) and life expectancy (Horváthová et al., 2021) of a street tree.

5 | CONCLUSIONS

After developing six typical urban shading types, we showed in our modelling study that daily and seasonal evapotranspiration rates of street trees were significantly influenced by those shading patterns. We demonstrated that shading types B–F had a significantly reduced water stress period in comparison to shading type A, regardless of initial soil moisture contents at the beginning of the vegetation period in the three case studies. Thus, trees in shading types B–F provided a longer lasting cooling function during dry periods later in the summer season due to higher evapotranspiration rates and a more effective shading function because of improved tree health. Based on these

results the next steps are the upscaling of shading types and water stress quantification to district and city scale by identifying the proportions of street trees that exhibit the six shading types and by estimating water supply or stress and ecosystem services of multiple street trees.

Several uncertainties remain regarding urban site conditions. A field campaign, which was guided by the modelling result, is on the way to substantiate the cascading effect of shading, direct and diffuse radiation, sap flow and soil moisture on diurnal to seasonal scales. In a long run, studies on water stress of street trees will aid to develop strategies for an effective irrigation management under a warming climate. A hypothesis for a future study might entail that with limited resources, shaded rather than exposed trees should be irrigated as they later retain their cooling function more efficiently in contrast to the former who transpire water and dry out rapidly.

AUTHOR CONTRIBUTIONS

Laura Tams: Conceptualization, investigation, methodology, visualization, writing—original draft. **Eva Paton:** Conceptualization; methodology; programming; writing—review; editing and funding acquisition. **Björn Kluge:** Conceptualization; methodology; writing—review; editing and funding acquisition.

ACKNOWLEDGEMENTS

This work was funded by the Deutsche Forschungsgemeinschaft (DFG) as part of the Urban Water Interfaces research training group (GRK 2032) and supported by the federal funding program 'Measures for adaptation to the consequences of climate change' of the Federal Ministry for the Environment, Nature Conservation, Nuclear Safety and Consumer Protection (BMUV) within the research project REWANKA. The authors are particularly grateful to Fred Meyer from the Chair of Climatology, TU Berlin, for providing diffuse radiation measurement equipment. Open Access funding enabled and organized by Projekt DEAL.

CONFLICT OF INTEREST STATEMENT

The authors have declared no conflict of interest for this article.

DATA AVAILABILITY STATEMENT

The data that support the findings of this study are available from the corresponding author upon reasonable request.

ORCID

Laura Tams https://orcid.org/0000-0003-2602-5612

REFERENCES

Adams, H. D., Luce, C. H., Breshears, D. D., Allen, C. D., Weiler, M., Hale, V. C., Smith, A. M. S., & Huxman, T. E. (2012). Ecohydrological consequences of drought- and infestation- triggered tree die-off: Insights and hypotheses. *Ecohydrology*, *5*(2), 145–159. https://doi.org/10.1002/eco.233

Alhassoun, R. (2009). Studies on factors affecting the infiltration capacity of agricultural soils. Zugl.: Braunschweig, Techn. Univ., Diss., 2009. Dissertationen aus dem Julius-Kühn-Institut. Quedlinburg: Julius Kühn-Inst. Bundesforschungsinst. für Kulturpflanzen.

Allen, R. G., Pereira, L. S., Raes, D., & Smith, M. (1998). Crop evapotranspiration: Guidelines for computing crop water requirements. FAO irrigation and drainage paper: Vol. 56. Rome: Food and Agriculture Organization of the United States.

Allen, R. G., Pruitt, W. O., Wright, J. L., Howell, T. A., Ventura, F., Snyder, R., & Elliott, R. (2006). A recommendation on standardized surface resistance for hourly calculation of reference ETo by the FAO56 Penman-Monteith method. *Agricultural Water Management*, *81*(1–2), 1–22. https://doi.org/10.1016/j.agwat.2005.03.007

Athamena, K., Sini, J.-F., Rosant, J.-M., & Guilhot, J. (2018). Numerical coupling model to compute the microclimate parameters inside a street canyon. *Solar Energy*, *170*, 470–485. https://doi.org/10.1016/j.solener.2018.05.015

Berthier, E., Dupont, S., Mestayer, P. G., & Andrieu, H. (2006). Comparison of two evapotranspiration schemes on a sub-urban site. *Journal of Hydrology*, *328*(3–4), 635–646. https://doi.org/10.1016/j.jhydrol.2006.01.007

Böhme, A., Wilhelm, T., & Golla, F. (2020). Hochhausleitbild für Berlin Qualität – Kompensation – Partizipation Mehrwerte für die Allgemeinheit. Retrieved from https://www.stadtentwicklung.berlin.de/planen/hochhausleitbild/download/Hochhausleitbild-fuer-Berlin_SenSW.pdf

Bowler, D. E., Buyung-Ali, L., Knight, T. M., & Pullin, A. S. (2010). Urban greening to cool towns and cities: A systematic review of the empirical evidence. *Landscape and Urban Planning*, *97*(3), 147–155. https://doi.org/10.1016/j.landurbplan.2010.05.006

Bréda, N., Huc, R., Granier, A., & Dreyer, E. (2006). Temperate forest trees and stands under severe drought: A review of ecophysiological responses, adaptation processes and long-term consequences. *Annals of Forest Science*, *63*(6), 625–644. https://doi.org/10.1051/forest:2006042

Chen, G., Wang, D., Wang, Q., Li, Y., Wang, X., Hang, J., Gao, P., Ou, C., & Wang, K. (2020). Scaled outdoor experimental studies of urban thermal environment in street canyon models with various aspect ratios and thermal storage. *The Science of the Total Environment*, *726*, 138147. https://doi.org/10.1016/j.scitotenv.2020.138147

David, A. A. J., Boura, A., Lata, J.-C., Rankovic, A., Kraepiel, Y., Charlot, C., Barot, S., Abbadie, L., & Ngao, J. (2018). Street trees in Paris are sensitive to spring and autumn precipitation and recent climate changes. *Urban Ecosystem*, *21*(1), 133–145. https://doi.org/10.1007/s11252-017-0704-z

Delta-T Devices. (2022). Sunshine pyranometer type SPN1: Data sheet. Retrieved from https://www.upgmbh.com/fileadmin/produkte/pdf/05119_rl0.pdf

Dickhaut, W., & Eschenbach, A. (Eds.) (2018). Entwicklungskonzept Stadtbäume: Anpassungsstrategien an sich verändernde urbane und klimatische Rahmenbedingungen. Hamburg: HafenCity Universität. Retrieved from http://edoc.sub.uni-hamburg.de/hcu/volltexte/2019/492/

Doninck, J. (2016). solarPos: Solar position algorithm for solar radiation applications: Calculation of solar zenith and azimuth angles. R-package Version 1.0. Retrieved from https://cran.r-project.org/web/packages/solarPos/solarPos.pdf

DWD Climate Data Center. (2022). Historical daily station observations for rainfall for Germany, version v007. Retrieved from https://cdc.dwd.de/portal

Gash, J. H. C. (1979). An analytical model of rainfall interception by forests. *Quarterly Journal of the Royal Meteorological Society*, *105*(443), 43–55. https://doi.org/10.1002/qj.49710544304

Gkatsopoulos, P. (2017). A methodology for calculating cooling from vegetation evapotranspiration for use in urban space microclimate simulations. *Procedia Environmental Sciences*, *38*, 477–484. https://doi.org/10.1016/j.proenv.2017.03.139

Gong, F.-Y., Zeng, Z.-C., Ng, E., & Norford, L. K. (2019). Spatiotemporal patterns of street-level solar radiation estimated using Google street view in a high-density urban environment. *Building and Environment*, *148*, 547–566. https://doi.org/10.1016/j.buildenv.2018.10.025

Grylls, T., & van Reeuwijk, M. (2021). Tree model with drag, transpiration, shading and deposition: Identification of cooling regimes and large-eddy simulation. *Agricultural and Forest Meteorology*, *298-299*, 108288. https://doi.org/10.1016/j.agrformet.2020.108288

Haase, D., & Hellwig, R. (2022). Effects of heat and drought stress on the health status of six urban street tree species in Leipzig, Germany. *Trees, Forests and People*, *8*, 100252. https://doi.org/10.1016/j.tfp.2022.100252

Hörnschemeyer, B., Henrichs, M., & Uhl, M. (2021). SWMM-UrbanEVA: A model for the evapotranspiration of urban vegetation. *Water*, 13(2), 243. https://doi.org/10.3390/w13020243

Horváthová, E., Badura, T., & Duchková, H. (2021). The value of the shading function of urban trees: A replacement cost approach. *Urban Forestry & Urban Greening*, *62*, 127166. https://doi.org/10.1016/j.ufug.2021.127166

Järvi, L., Grimmond, C., & Christen, A. (2011). The surface urban energy and water balance scheme (SUEWS): Evaluation in Los Angeles and Vancouver. *Journal of Hydrology*, *411*(3–4), 219–237. https://doi.org/10.1016/j.jhydrol.2011.10.001

Johnson, G. T., & Watson, I. D. (1984). The determination of view-factors in urban canyons. *Journal of Climate and Applied Meteorology*, *23*(2), 329–335. https://doi.org/10.1175/1520-0450(1984)023<0329:TDOVFI>2.0.CO;2

Kirmaier, M. (2020). Small leaved lime sitting on the dry: Effects on evapotranspiration, leaf area and vitality (master thesis). Technische Universität Berlin, Berlin.

Kottek, M., Grieser, J., Beck, C., Rudolf, B., & Rubel, F. (2006). World map of the Köppen-Geiger climate classification updated. *Meteorologische Zeitschrift*, *15*(3), 259–263. https://doi.org/10.1127/0941-2948/2006/0130

Masson, V. (2000). A physically-based scheme for the urban energy budget in atmospheric models. *Boundary-Layer Meteorology*, *94*(3), 357–397. https://doi.org/10.1023/A:1002463829265

McDowell, N., Pockman, W. T., Allen, C. D., Breshears, D. D., Cobb, N., Kolb, T., Plaut, J., Sperry, J., West, A., Williams, D. G., Yepez, E. A., & Yepez, E. A. (2008). Mechanisms of plant survival and mortality during drought: Why do some plants survive while others succumb to drought? *The New Phytologist*, *178*(4), 719–739. https://doi.org/10.1111/j.1469-8137.2008.02436.x

Mei, S.-J., & Yuan, C. (2022). Urban buoyancy-driven air flow and modelling method: A critical review. *Building and Environment*, *210*, 108708. https://doi.org/10.1016/j.buildenv.2021.108708

Olmedo, G., Ortega-Farías, S., Fuente-Sáiz, D., Luego, D., & Fuentes-Peñailillo, F. (2016). Water: Tools and functions to estimate actual evapotranspiration using land surface energy balance models in R. *The R Journal*, *8*(2), 352. https://doi.org/10.32614/RJ-2016-051

Pace, R., de Fino, F., Rahman, M. A., Pauleit, S., Nowak, D. J., & Grote, R. (2021). A single tree model to consistently simulate cooling, shading, and pollution uptake of urban trees. *International Journal of Biometeorology*, *65*(2), 277–289. https://doi.org/10.1007/s00484-020-02030-8

Pallasch, M., Geisler, D., & Kluge, B. (2022). Straßenbäume und dezentrale Versickerung als Beitrag wassersensibler Stadtentwicklung. *Teil*, *2*(9), 747–759. https://doi.org/10.3242/kae2022.09.001

R Core Team. (2021). R: A language and environment for statistical computing (version 4.1.2) [computer software]. Vienna, Austria: R Foundation for Statistical Computing: R Foundation for Statistical Computing. s

Rahman, M. A., Moser, A., Rötzer, T., & Pauleit, S. (2017). Microclimatic differences and their influence on transpirational cooling of Tilia cordata in two contrasting street canyons in Munich, Germany. *Agricultural and Forest Meteorology*, *232*, 443–456. https://doi.org/10.1016/j.agrformet.2016.10.006

Revelli, R., & Porporato, A. (2018). Ecohydrological model for the quantification of ecosystem services provided by urban street trees. *Urban Ecosystem*, *21*(3), 489–504. https://doi.org/10.1007/s11252-018-0741-2

Robineau, T., Rodler, A., Morille, B., Ramier, D., Sage, J., Musy, M., Graffin, V., & Berthier, E. (2022). Coupling hydrological and microclimate models to simulate evapotranspiration from urban green areas and air temperature at the district scale. *Urban Climate*, *44*, 101179. https://doi.org/10.1016/j.uclim.2022.101179

Ross, J. (1981). Incident radiation. In J. Ross (Ed.), *The radiation regime and architecture of plant stands* (pp. 159–174). Springer Netherlands. https://doi.org/10.1007/978-94-009-8647-3_10

Rötzer, T., Moser-Reischl, A., Rahman, M. A., Hartmann, C., Paeth, H., Pauleit, S., & Pretzsch, H. (2021). Urban tree growth and ecosystem services under extreme drought. *Agricultural and Forest Meteorology*, *308-309*, 108532. https://doi.org/10.1016/j.agrformet.2021.108532

Rötzer, T., Rahman, M. A., Moser-Reischl, A., Pauleit, S., & Pretzsch, H. (2019). Process based simulation of tree growth and ecosystem services of urban trees under present and future climate conditions. *The Science of the Total Environment*, *676*, 651–664. https://doi.org/10.1016/j.scitotenv.2019.04.235

Schütt, A., Becker, J. N., Gröngröft, A., Schaaf-Titel, S., & Eschenbach, A. (2022). Soil water stress at young urban street-tree sites in response to meteorology and site parameters. *Urban Forestry & Urban Greening*, *75*, 127692. https://doi.org/10.1016/j.ufug.2022.127692

SenUVK. (2018). Bodengesellschaften und Bodenarten 2015. Senatsverwaltung für Stadtentwicklung, Bauen und Umwelt. Retrieved from https://daten.berlin.de/datensaetze/bodengesellschaften-und-bodenarten-2015-umweltatlas-wfs

SenUVK. (2021). Straßenbaum-Zustandsbericht Berliner Innenstadt 2020: Ergebnisse der Straßenbaum-Zustandserhebung aus CIR Luftbildern. Berlin. Retrieved from https://www.berlin.de/sen/uvk/_assets/natur-gruen/stadtgruen/stadtbaeume/strassen-und-parkbaeume/zustand-der-strassenbaeume/strb_zustandsbericht2020.pdf

Smets, V., Wirion, C., Bauwens, W., Hermy, M., Somers, B., & Verbeiren, B. (2019). The importance of city trees for reducing net rainfall: Comparing measurements and simulations. *Hydrology and Earth System Sciences*, *23*(9), 3865–3884. https://doi.org/10.5194/hess-23-3865-2019

Timm, A., Kluge, B., & Wessolek, G. (2018). Hydrological balance of paved surfaces in moist mid-latitude climate – A review. *Landscape and Urban Planning*, *175*, 80–91. https://doi.org/10.1016/j.landurbplan.2018.03.014

Vico, G., Revelli, R., & Porporato, A. (2014). Ecohydrology of street trees: Design and irrigation requirements for sustainable water use. *Ecohydrology*, *7*(2), 508–523. https://doi.org/10.1002/eco.1369

Wang, C., Wang, Z.-H., & Ryu, Y.-H. (2021). A single-layer urban canopy model with transmissive radiation exchange between trees and street canyons. *Building and Environment*, *191*, 107593. https://doi.org/10.1016/j.buildenv.2021.107593

Wessolek, G., Kaupenjohann, M., & Renger, M. (2009). *Bodenökologie und Bodengenese. Bodenphysikalische Kennwerte und Berechnungsverfahren für die Praxis. Bodenökologie und Bodengenese* (Vol. 40). Technische UNiversität Berlin.

Wessolek, G., & Kluge, B. (2021). Predicting water supply and evapotranspiration of street trees using hydro-pedo-transfer functions (HPTFs). *Forests*, *12*(8), 1010. https://doi.org/10.3390/f12081010

How to cite this article: Tams, L., Paton, E. N., & Kluge, B. (2023). Impact of shading on evapotranspiration and water stress of urban trees. *Ecohydrology*, *16*(6), e2556. https://doi.org/10.1002/eco.2556

APPENDIX A

TABLE A1 URbanTRee model equations.

Eq	Process	Function	Unit
4	Potential evapotranspiration(ET_p)	$ET_p = \frac{0.408\Delta(R_G - G) + \gamma \frac{C_n}{T+273} u_2 (e_s - e_a)}{\Delta + \gamma(1 + c_d * c_u)}$ R_G = *global radiation at the tree surface* $(W\,m^{-2})$ G = *soil heat flux density* $(MJ\,m^{-2})$ T = *air Temperature at 2m height* $(^\circ C)$ u_2 = *wind speed at 2 m height* $(m\,s^{-1})$ e_s = *saturation vapour pressure* (kPA) e_a = mean actual vapor pressure at 1.5 to 2.5 m height kPa Δ = *slope of the saturation vapour pressure − temperature curve* $\left(kPa^\circ C^{-1}\right)$ γ = *psychrometric constant* $\left(kPa^\circ C^{-1}\right)$ C_n = *numerator constant* $\left(K\,mm\,s^3 Mg^{-1} h^{-1}\right)$ C_d = *denominator constant* $(s\,m^{-1})$	mm
5	Interception (I)	$I = \begin{cases} 0 & for \sum I_{last\ 5\,h} > Imax \\ P * c_I * c_P & for\ I < I_{max}\ and \sum I_{last\ 5\,h} < Imax \\ I_{max} & for\ I > I_{max} \end{cases}$ P = *Precipitaiton* (mm) c_I = *Interception coefficient* $(\%)$ c_P = *pheno − multiplier* $(\%)$ I = *Interception* (mm) I_{max} = *threshold cumulative interception storage* (mm) $I_{last\ 5\,h}$ = *cumulative interception of the last 5 hours* (mm)	mm
6	Runoff (R)	$R = \begin{cases} 0 & for\ P < c_{TR} \\ (P - I) * c_R & for\ P > c_{TR} \end{cases}$ c_R = *Runoff coefficient* c_{TR} = *Runoff threshhold coefficent* (mm)	mm
7	Infiltration (In)	$In = \begin{cases} (P - I - R) & for\ P - I - R < c_{In} \\ c_{In} & for\ P - I > c_{In} \end{cases}$ R = *Runoff* (mm) c_{In} = *Infiltration coefficient* $\left(mm\,h^{-1}\right)$	m
8	Change in soil water content (ΔS)	$\frac{\Delta S}{\Delta t} = In - ET_a - Per$ ΔS = *Change in soil water content of* (mm) Δt = *Time step* $(hours)$ In = *Infiltration* (mm) ET_a = *Actual evapotranspiration* (mm) Per = *Percolation* (mm)	mm
9	Actual evapotranspiration for wet conditions (ET_{ax})	$ET_{ax} = c_P * K_C * ET_p$ ET_p = *potential evapotranspiration* (mm) K_C = *Crop coefficient* c_P = *pheno − multeplier* $(\%)$	
10	Actual evapotranspiration (ET_a)	$ET_a = \begin{cases} 0 & for\ S_i - PWP \le 0 \\ K_{EA} * ET_{ax} & for\ S_i < PWP + K_S * nFK \\ S_i - PWP & for\ S_i - PWP \le ET_{ax} \\ ET_{ax} & for\ all\ other\ wet\ conditions \end{cases}$ K_{EA} = *ETA reduction coefficient during water stress* $(\%)$ ET_{ax} = *actual evapotranpiration for wet conditions* (mm) S_i = *soil moiture of current time step* (mm) K_S = *Water stress coefficient* $(\%)$ nFK = *plant available water* $(FK - PWP, mm)$ PWP = *permanent wilting point* (mm) FK = Field capacity (mm)	mm
11	Percolation (Per)	$Per = \begin{cases} 0 & for\ S_i < FK \\ S_i - FK & for\ S_i > FK \end{cases}$ S_i = *Soil water content of previous timestep* (mm)	mm

TABLE A2 Parameterization values for URbanTRee model.

Parameter	Unit	Value used in model	Values from literature
Runoff threshold (c_{TR})	mm	Sealed soil with asphalt: 3 Open soil: 10	Timm et al., 2018
Runoff coefficient (c_R)	[−]	Sealed soil with asphalt: 0.9 Open soil: 0.2	Timm et al., 2018
Infiltration rate (c_{In})	mmh^{-1}	Sealed soil with asphalt: 1 mm Open soil: 20 mm	Alhassoun, 2009
Threshold cumulative interception storage (I_{max})	mm	10 mm	Numerical control parameter
Interception coefficient (c_I)	[−]	0.5	Smets et al., 2019
Pheno-multiplier (c_P)	[−]	$c_P = \begin{cases} 0 & for\ DOY < 100 \\ 0.5 & for\ 100 < DOY > 114 \\ 1 & for\ 114 < DOY > 260 \\ 0.5 & for\ 260 < DOY > 274 \\ 0 & for\ DOY > 274 \end{cases}$ $DOY = Day\ of\ the\ year$	Derived from: Allen et al., 1998; Wessolek & Kluge, 2021
Crop coefficient (K_C)	[−]	1.6	Wessolek & Kluge, 2021
Water stress coefficient (K_{EA})	[−]	0.5	Derived from: Allen et al., 1998; Pallasch et al., 2022
Water stress factor (K_S)	[−]	0.3	Derived from: Allen et al., 1998; Pallasch et al., 2022
Tree crown area	m^2	16	Wessolek & Kluge, 2021
Tree rooting depth	m	1.5	Wessolek & Kluge, 2021
Field capacity (FK)	m^3m^{-3}	26 (for a loamy sand)	Wessolek et al., 2009
Permanent wilting point (PWP)	m^3m^{-3}	10 (for a loamy sand)	Wessolek et al., 2009
Shading types	—	A, B, C, D, E, F	See methods Figure 5
Sky view factor	—	0.3 for type B 0.5 for types C–F 1 for type A	Wessolek & Kluge, 2021
Soil sealing	—	Open soil (100%), sealed soil (100%)	Assumption